Journal of Marine Systems 129 (2014) 405–414

Contents lists available at ScienceDirect

Journal of Marine Systems

journal homepage: www.elsevier.com/locate/jmarsys

Tropical storm-induced turbulent mixing and chlorophyll-*a* enhancement in the continental shelf southeast of Hainan Island

Shuwen Zhang [a], Lingling Xie [a,*], Yijun Hou [b], Hui Zhao [a], Yiquan Qi [c], Xiaofei Yi [a]

[a] Guangdong Key Lab. of Climate, Resource and Environment in Continental Shelf Sea and Deep Sea, College of Ocean and Meteorology, Guangdong Ocean University, Zhanjiang 524088, China
[b] Institute of Oceanology, Chinese Academy of Sciences, Qingdao 266003, China
[c] State Key Lab. of Tropical Oceanography, South China Sea Institute of Oceanology, Guangzhou 510301, China

ARTICLE INFO

Article history:
Received 14 March 2013
Received in revised form 30 August 2013
Accepted 2 September 2013
Available online 6 September 2013

Keywords:
Tropical storm
Near-inertial oscillation
Turbulent mixing
Chlorophyll concentration
Ocean current observations

ABSTRACT

Based on moored observations and remote sensing data in July and August 2005, energy sources for enhancing turbulent mixing and possible mechanisms of phytoplankton bloom in the continental shelf southeast of Hainan Island under the influence of Washi, a fast-moving and weak tropical storm, are analyzed in this paper. Observations show that strong near-inertial internal waves were generated by the rapidly changing wind stress and the near-inertial energy was dissipated quickly across the thermocline. The strong turbulent mixing associated with the near-inertial baroclinic shear instability occurred with maximum eddy diffusivity above 3.2×10^{-4} m^2 s^{-1}, and the surface chlorophyll-*a* (Chl-*a*) concentration after the storm increased by 22.2%. The Chl-*a* concentration augment was inferred to be an upper ocean biophysical response to the enhanced near-inertial turbulent mixing which could increase the upward nutrient flux into the surface low eutrophic zone during the passage of Washi.

1. Introduction

The upper ocean response to a moving storm or hurricane has been an important topic in the physical oceanography study (D'Asaro, 2003; Price, 1981; Sanford et al., 2011; Shay et al., 1992; Zedler et al., 2002; Zheng et al., 2006) and drawn more and more attention for recent years (Black and Dickey, 2008; Dohan and Davis, 2011; Lee and Brink, 2010; Lin et al., 2003; Wada et al., 2009; Walker, 2005; Wang et al., 2012). The response of the upper ocean to a storm or hurricane is shown by sea surface temperature cooling and near-inertial oscillations that are strong on the right of the storm track. The storm-induced near-inertial oscillations play an important role in mass, heat and energy exchanges between the upper mixed-layer and deep layer below the pycnocline. Near-inertial internal waves are not only a carrier for the kinetic energy being transported to the ocean interior (Zhou et al., 2005) but also a driving force for heat being fluxed down to the low layer of ocean water (Sriver and Huber, 2007). The influence of tropical storms on the nutrient flux from the water below thermocline to the mixed-layer is insignificant for the deep ocean area. In the continental shelf sea, however, the situation changes because the near-inertial internal waves induced by tropical storms may directly affect the ocean water below thermocline and enhance shear and turbulent mixing (Burchard and Rippeth, 2009; Rippth et al., 2002; Shearman, 2005), leading to the increase of the vertical nutrient flux. Consequently, high primary production appears in euphotic zones. Thus, studies on the near-inertial internal waves and phytoplankton blooms caused by tropical storms are crucial in understanding the mixing dynamics and biogeochemical processes in continental shelf seas.

The South China Sea (SCS) with an area of about 34,500 km^2 is the largest marginal sea in the western Pacific. It is susceptible to tropical storms averaging up to 15 occurrences per year according to historical records (Lin et al., 2003; Wu et al., 2005; Zhao et al., 2008). As a tropical storm passes by, the upper ocean has significant response to the strong wind forcing (J. Chang et al., 2008, Y. Chang et al., 2008; Lin et al., 2008; Shang et al., 2008), with nutrients efficiently replenished in euphotic layer and phytoplankton biomass rapidly enhanced (Lin et al., 2003; Shiah et al., 2000; Zhao et al., 2009). Most of the area of the SCS has sufficient sunshine but is short of nutrients, and the nutrient supply becomes a main factor sustaining the primary production (Tang et al., 2004a, 2004b). Recent studies show that tropical storms or typhoons are very important in forcing the promotion of phytoplankton biomass and primary production (Lin et al., 2003; Zheng and Tang, 2007). However, previous studies mainly focus on the influence of strong typhoons on primary production in the SCS (Lin et al., 2003; Sun et al., 2010; Zhao et al., 2008; Zheng and Tang, 2007). Little work has been done on the influence of weak tropical storms, especially on the correlation between the turbulent mixing induced by storm-generated near-inertial oscillations and the biological process of phytoplankton blooming.

* Corresponding author at: College of Ocean and Meteorology, Guangdong Ocean University, Zhanjiang 524088, China. Tel.: +86 759 2396037; fax: +86 759 2396055.
E-mail address: llingxie@163.com (L. Xie).

0924-7963
http://dx.doi.org/10.1016/j.jmarsys.2013.09.002

In fact, it is not easy to make in-situ observations on the ocean responses to tropical storms. Satellite remote sensing of sea surface temperature, wind speed, and ocean color has been proven to be a key measure for understanding the ocean response to tropical storms. However, the remote sensing only provides ocean surface data and in-situ profile observations are necessary to disclose the detailed storm-related oceanic variability. Up to now, few existing datasets are appropriate for unveiling the upper ocean physical processes under the tropical storm influence in the continental shelf region of the SCS (Cui et al., 2009; Sun et al., 2011), especially in the area off the Hainan Island.

This study presents moored observations of ocean responses to a weak tropical storm in the continental shelf region off Hainan Island. The in-situ observations combining with multi-sensor remote sensing data during the tropical storm are used to investigate the influence of the tropical storm on phytoplankton distribution and the dynamical mechanism of the phytoplankton bloom. These investigations help to better understand upper ocean physical and biological processes in response to the tropical storm Washi which passed the northwestern shelf of the SCS in 2005.

2. Data and method

2.1. Remote sensing data

The typhoon track data used in this study are obtained from the Unisys Weather website (http://weather.unisys.com/hurricane/w_pacific/), which is based on the best hurricane track data issued by the Joint Typhoon Warning Center (JTWC). The data include maximum sustained surface wind speeds and the storm center locations every 6 h. The moving speed of a storm was thus estimated based on the positions of its center every 6 h in our analysis. The tropical storm Washi was formed as a cyclone in the northwestern SCS (18.4°N, 112.6°E) at 18:00 on July 28, 2005. It became a tropical storm on July 29 and reached its maximum wind speed of 23.1 m s^{-1} on July 30. Then, Washi reduced to a cyclone and made the landfall in the coast of northeast Vietnam (20.5°N, 104.5°E) on July 31 (Fig. 1). The storm with wind speed less than 18 m s^{-1} moved slowly in its first 18 h (<2.5 m s^{-1}) and then fast with a high speed (>3.7 m s^{-1}). Generally, the tropical storm Washi was a fast-moving, weak storm.

Daily sea surface temperature (SST) data are derived from the Tropical Rainfall Measuring Mission (TRMM) Microwave Imager (TMI) with a spatial resolution of 0.25° by 0.25°. Because of the cloud-penetration capability of TMI, the measurements can overcome the cloudiness influence (Wentz et al., 2000). Surface wind data were obtained from the South China Sea Ocean Data Base (SCSDB, http://www.ocdb.csdb.cn/), which is an reanalysis product of the National Ocean and Meteorology Administration (NOAA) Earth System Research Laboratory (ESRL) survey data. The spatial resolution of the wind data is 0.25° by 0.25° and the temporal resolution is 6 h. The chlorophyll data are derived from MODIS-Aqua data (http://gdata1.sci.gsfc.nasa.gov) with the spatial resolution of 9 km × 9 km.

2.2. Moored observations

A moored observation system had been deployed at (19°35′N, 112°E) in the northwest SCS for 6 days from July 28 to August 2, 2005 by the Institute of Oceanology, Chinese Academy of Sciences. The depth of the mooring site is 130 m, about 130 km away from the nearest center of

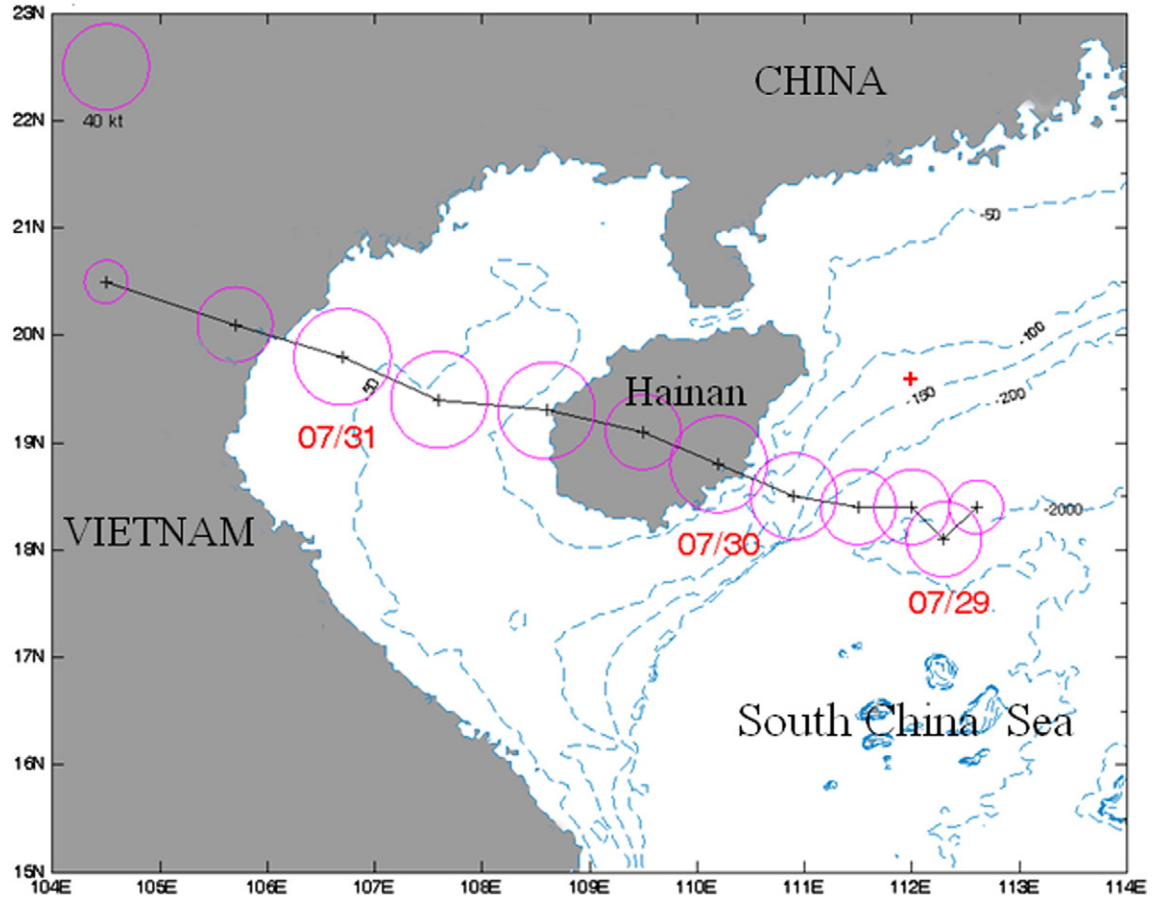

Fig. 1. Map of the study area, where the plus sign indicates the mooring position, and the red circles denote the track locations of the tropical storm Washi.

Washi (Fig. 1). A downward looking 190 kHz Acoustic Doppler Current Profiler (ADCP) was used to sample current velocity at a total of 51 layers from 14 m to 114 m depth with an interval of 2 m every 10 min. Temperature profile data were also collected every 10 min by using a chain of temperature sensors at the depths from 4 m to 75 m with an interval of 1 m.

2.3. Data processing and methods

The SCSDB wind data at the grid of the mooring station are used as the storm forcing winds (Fig. 2a). The time series of ocean current velocity and temperature profiles are directly from the moored observations (Fig. 2b–d). Thermocline is defined as the depth with temperature gradient higher than 0.2 °C m^{-1}. Baroclinic velocity profiles with 2 m interval are derived by subtracting the vertical velocity means, namely the barotropic velocities from the observed velocity profiles. Power spectra of baroclinic velocities at all the depth layers are obtained with periodogram method (Fig. 5), and the temporal variation of current component at a certain frequency is inferred by continuous wavelet transform (CWT) method with Morlet wavelet (Fig. 6). Near-inertial baroclinic velocities within [0.8 f–1.25 f] are extracted by using a second-order Butterworth filter applied in the time domain (Fig. 7). The filter is applied twice, firstly forward and then backward to minimize the phase distortion. After that, the inertial shear $S_f^2 = \left(\frac{\partial u_f}{\partial z}\right)^2 + \left(\frac{\partial v_f}{\partial z}\right)^2$ with 2 m vertical resolution is calculated.

Since there were no simultaneous salinity observations with the temperature, the mean of climatological salinity profiles in July–August within 10 km around the mooring station from World Ocean Database 2009 (WOD09, http://www.nodc.noaa.gov/OC5/WOD/datageo.html) is used to represent the background salinity at the mooring location. The observed temperature profiles (with 1 m vertical resolution) are smoothed with 5 m moving window and then are averaged to generate 2 m vertical grids. Then, 2 m grids of bouncy frequency N are calculated from the density profiles with observed temperature and WOD09 salinity data.

The energy dissipation rate can be derived from fine-scale parameterization that characterizes the relationship among density gradient, velocity shear, and energy dissipation. Among several existing turbulent models (e.g., Palmer et al., 2013), the parameterization scheme proposed by MacKinnon and Gregg (2003) (MG03 hereafter) has been successfully used to describe continental shelf mixing induced by near-inertial oscillations (e.g., Mackinnon and Gregg, 2005; Palmer et al., 2008; van der Lee and Umlauf, 2011). As discussed in the following sections, near-inertial oscillations are dominant at the mooring station after the storm (Figs. 5–7) and the wind is further verified to play an important role in shear augment (Fig. 9). The parameterization of MG03 is thus appropriate to infer mixing in this study. It is given by

$$\varepsilon = \varepsilon_0 (N/N_0)\left(S_{lf}/S_0\right), \tag{1}$$

where ε is the energy dissipation rate; N is the buoyancy frequency; S_{lf} is the low-frequency shear of background velocity that resulted from large-scale waves (e.g. near-inertial internal waves); $N_0 = S_0 = 3$ cph; and $\varepsilon_0 = 10^{-8}$ Wkg^{-1}. The turbulent eddy diffusivity κ_ρ is calculated from the dissipation rate ε and the buoyancy frequency N by (Osborn, 1980):

$$\kappa_\rho = 0.2\varepsilon/N^2. \tag{2}$$

3. Results

3.1. Upper ocean temperature and velocity response to tropic storm Washi

As shown in Fig. 2a, the wind speed at the mooring station was 5–8 m s^{-1} before July 29, and increased dramatically to 18.9 m s^{-1} on July 30 when the storm was passing by, and then decreased rapidly below 10 m s^{-1} on August 1 after the storm passage. Fig. 3 shows the temporal-spatial distribution of SST during the storm and reveals that the sea surface cooled down substantially along the track of Washi and a distinct, low temperature center (<27 °C) appeared to southeast of Hainan Island on July 30–31; the low temperature water extended northward from July 29 to 31 and the cooling minimum occurred to southwest of the mooring station on July 31. The SST at the mooring location was high (>30 °C) on July 27–28 prior to the storm, dramatically decreased on July 29, reached the minimum of 27.5 °C on July 31, and then warmed up after the storm. Meanwhile, the observed temperature profiles show that the mixed layer apparently deepened with the temperature cooling from 30 °C to 28 °C (Fig. 2b). As the wind weakened after the storm, the observed current velocity tended to increase (Fig. 2c–d), and obviously, the magnitude and direction of the velocity varied periodically in a cycle of about 35 h with the inertial frequency at the mooring location.

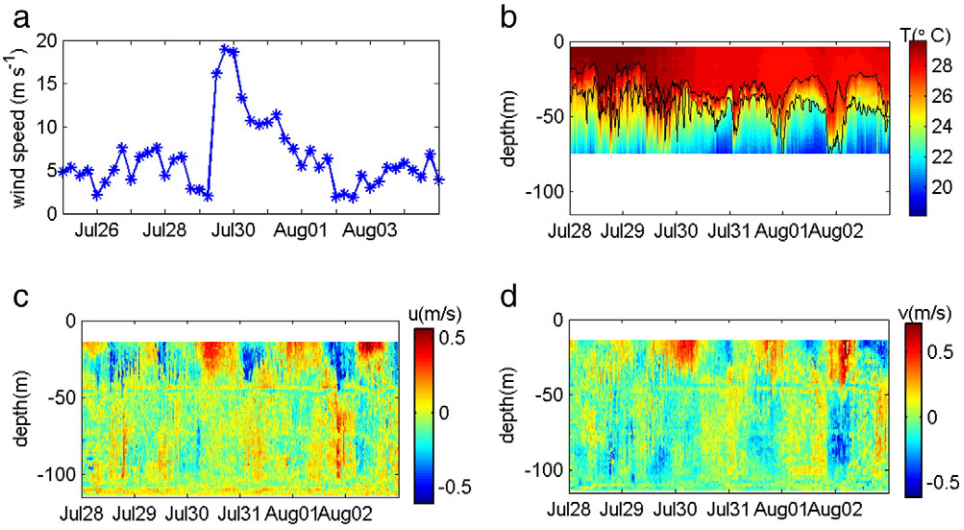

Fig. 2. The wind speed around the mooring location (a) and the observed temperature profiles (b), the east component (c) and north component (d) of velocity profiles at the mooring station. The black lines in (b) indicate the thermoclines.

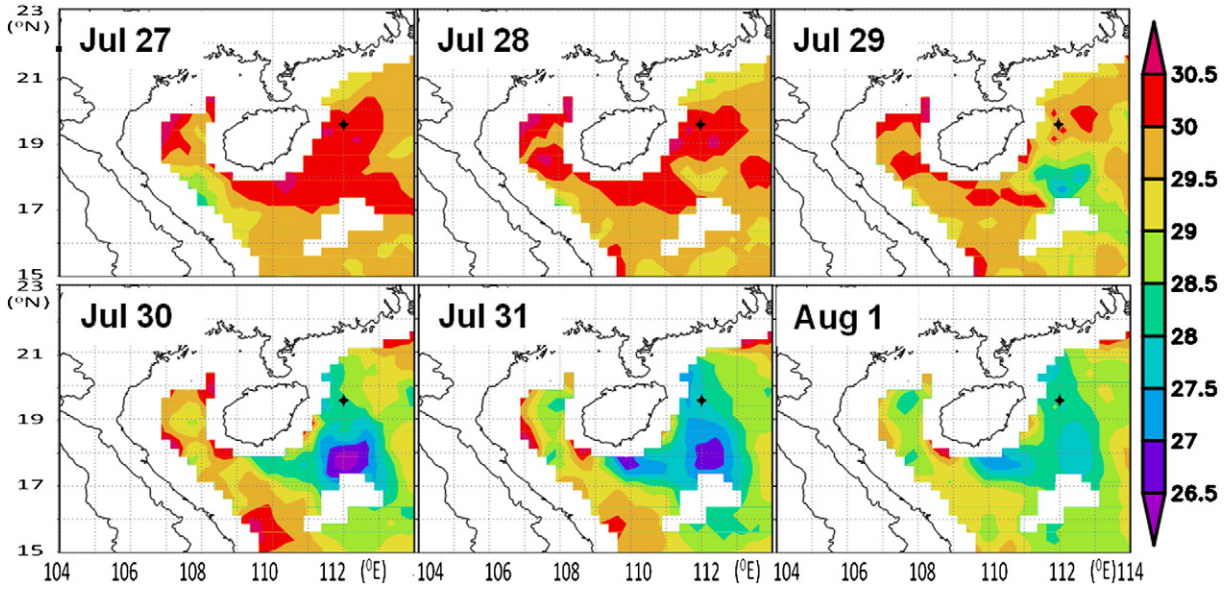

Fig. 3. Sea surface temperature derived from TRMM in the study area during July and August, 2005. The black plus sign indicates the mooring station.

3.2. Storm-induced near inertial oscillations and turbulent mixing

The barotropic kinetic energy and the vertical mean of the baroclinic kinetic energy at the mooring location are shown in Fig. 4. For the whole period during the Washi passage, the baroclinic energy had dominated the barotropic and increased dramatically on August 2. The power spectra of the baroclinic velocity are derived, revealing the existence of dominant near inertial oscillations almost in the whole water depth (Fig. 5). This is different from the near-inertial slab motion confined in surface mixed layer in open ocean (e.g. D'Asaro, 2003). Further analysis with wavelet transform method shows that oscillations at near-inertial period appear and dominate on Jul 31–August 2 after the storm both in the upper mixed layer (14 m) and deeper layer below the thermocline (70 m), though the oscillation below thermocline is relatively weaker and a little time-delayed than that in the upper mixed layer (Fig. 6). The near-inertial oscillations with the frequency range of 0.8–1.25*f* are then extracted and shown in Fig. 7. We can see that strong near-inertial internal waves with a period of about 35 h and a maximum velocity above 0.2 m s^{-1} were induced by Washi, especially on days after July 30 when the wind speed decreased rapidly. The directions of the near-inertial velocities in the upper mixed layer and that in deep part are definitely opposite (Fig. 7a, b), indicating a 180° phase shift across the thermocline. This phase shift has commonly been found for inertial oscillation in coastal ocean due to the proximity of the coastline and the resulting pressure gradient (e.g., Rippth et al., 2002). The kinetic energy of the near-inertial internal waves has two peaks in depth, one at the mixed layer above 30 m, and the other at depth of about 50–100 m below the thermocline (Fig. 7c). The energy maximum appeared on July 31–August 1 in the mixed layer with value above 0.04 m^2 s^{-2}, while the minimum close to zero displays near the thermocline bottom at 40–50 m depth. The other near-inertial energy peak below thermocline reaches less than 0.01 m^2 s^{-2}, much smaller than the peak in the mixed layer.

Near-inertial internal waves induced by a storm play an important role in the wind energy input into the ocean interior (Zhou et al., 2005). As shown in Fig. 8, the anticyclonic spectrum is dominant in the rotary wave-number spectra of the near-inertial oscillations at the mooring location, indicating that the near-inertial energy gained from the storm fluxed downward in the whole period of the storm event. The downward transport of energy became higher on July 30 and 31 when the storm wind decreased rapidly (Fig. 8). The energy input from wind forcing into the ocean is distributed to different modes of ocean motions, and part of energy input is dissipated at the bottom of the mixed layer and in the thermocline, and the rest penetrates the thermocline to the lower layer waters (D'Asaro et al., 1995). The near-inertial internal waves may dissipate the input energy by means of the wave–wave interaction, wave–current interaction, and meso-scale processes (Chant, 2001; Jacob and Shay, 2003), and the mixed layer depth also affects the downward energy flux (Shearman, 2005). According to Alford and Gregg (2001), the kinetic energy of near-inertial internal waves reaches maximum in the mixed layer, but decreases rapidly after penetrating the thermocline. In our observations, the kinetic energy of the near-inertial internal waves obviously decreased with depth in the mixed layer (Fig. 7d), and only about 11.5% of the energy of the

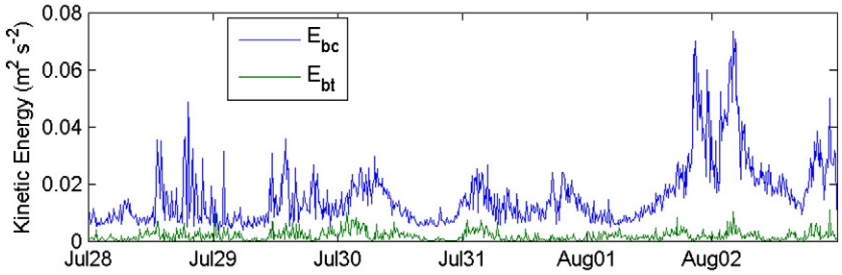

Fig. 4. The barotropic kinetic energy (green line) and the vertically-averaged baroclinic kinetic energy (blue line) at the mooring location.

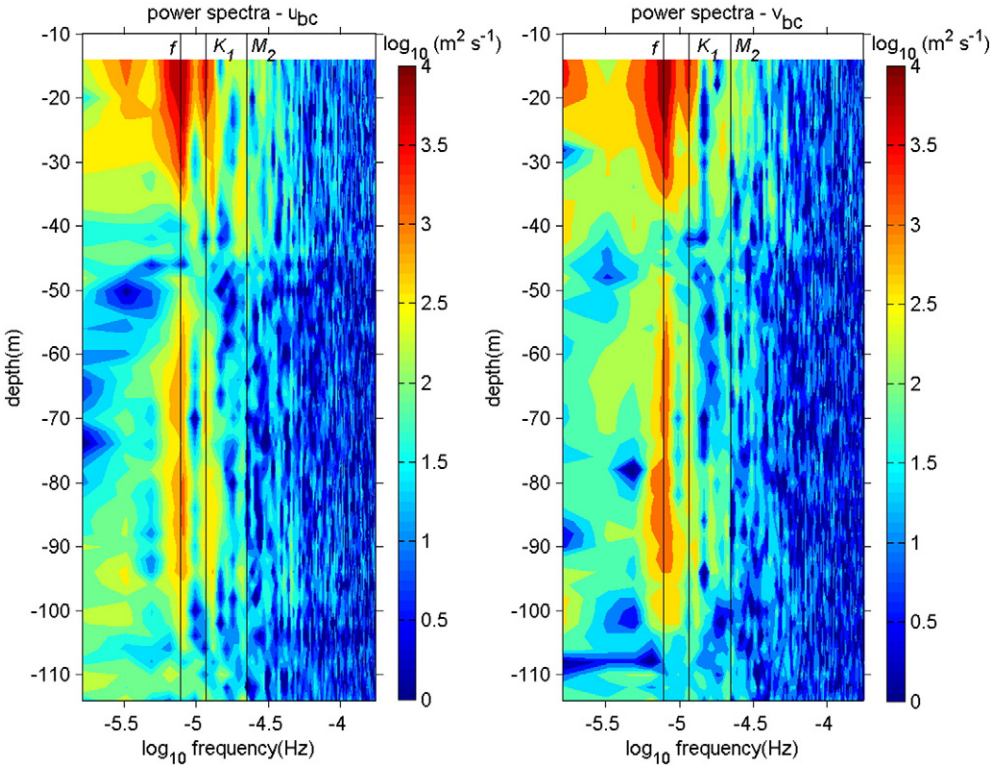

Fig. 5. The power spectra of baroclinic velocities. The three black lines indicate the inertial (f), diurnal (K_1) and semidiurnal (M_2) frequencies.

upper 30 m depth entered the water below 50 m. This result is consistent with the observations by Alford and Gregg (2001). The 180° phase shift of inertial velocities is a potentially significant source in driving shear instability and therefore mixing to dissipate the inertial energy across the thermocline (Rippth, 2005).

Burchard and Rippeth (2009) developed a simple analytical model to investigate the mechanism for generation of enhanced shear across the thermocline. According to their two-layer model which ignores lateral density gradient, advection and mixing, the variance of the bulk shear between the upper and deeper flows separated by strongest

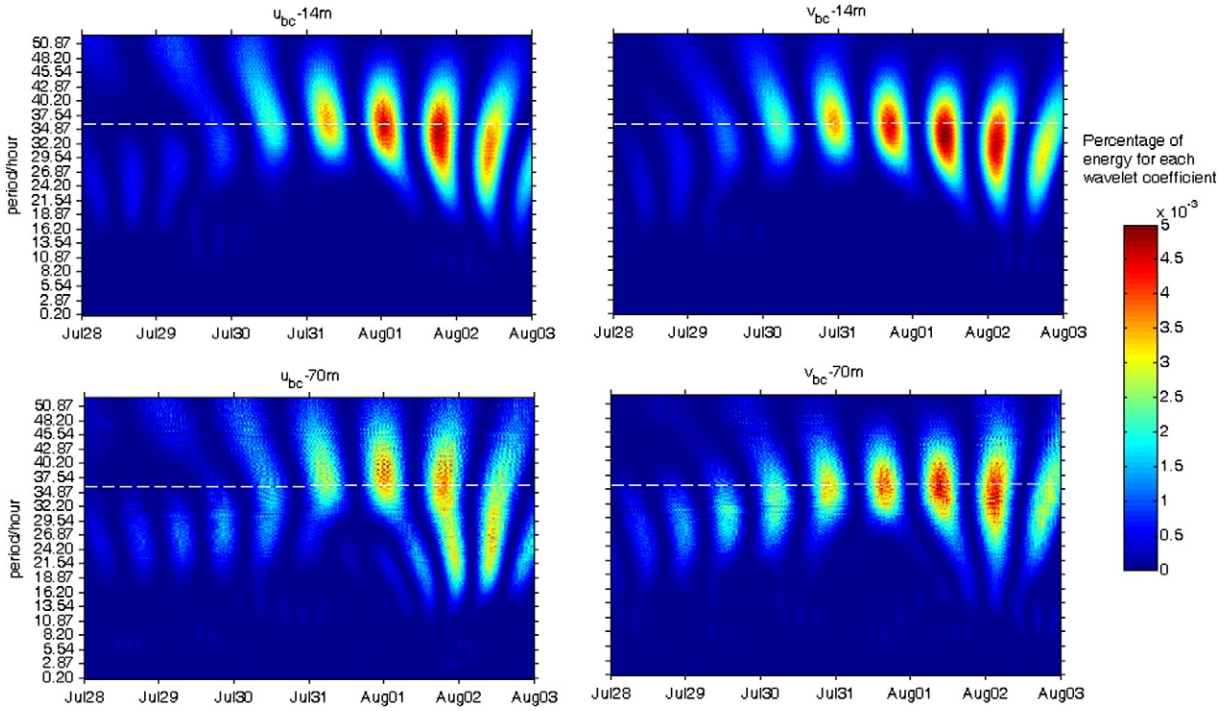

Fig. 6. Temporal variation of energy at different periods (frequencies) for baroclinic velocities at 14 m and 70 m by CWT method. The white dash line indicates the local inertial frequency.

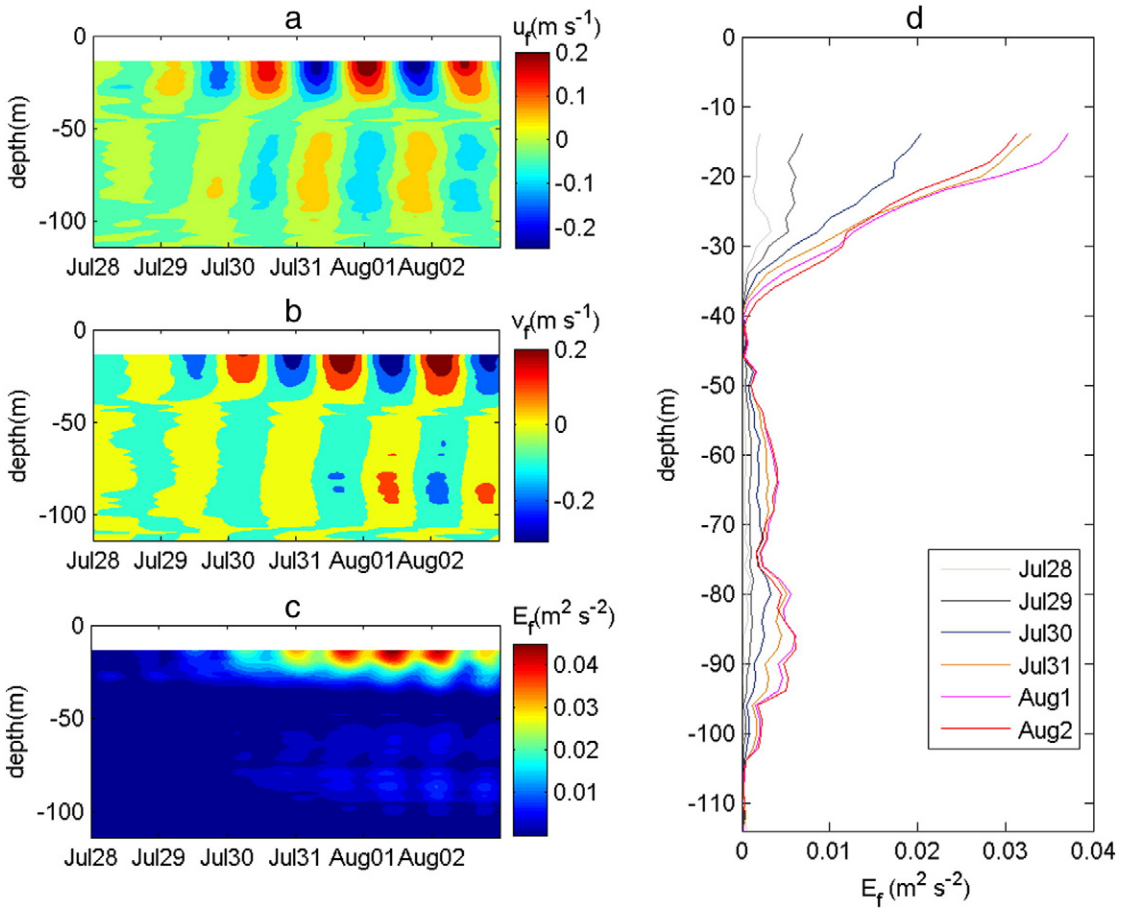

Fig. 7. The profiles of zonal near-inertial velocity u_f (a), meridional near-inertial velocities v_f (b), and near-inertial kinetic energy E_f (c) as well as the daily-averaged near-inertial kinetic energy (d).

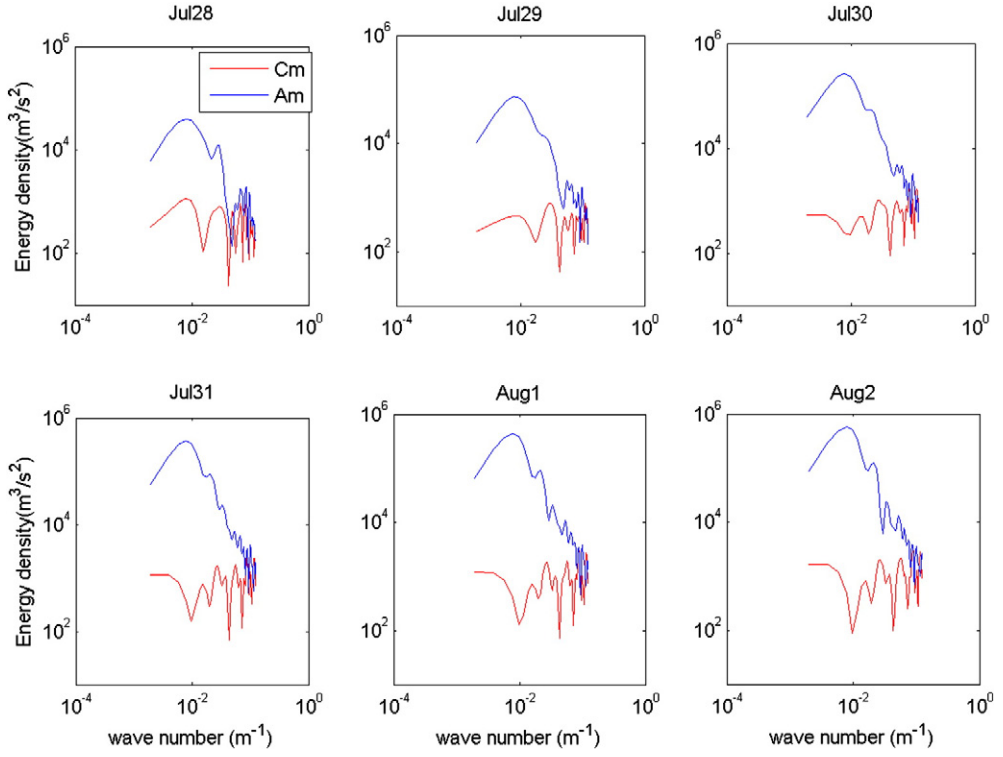

Fig. 8. Daily-averaged vertical wave-number rotary spectra of near-inertial internal wave. The blue lines indicate the anticyclonic spectra and red lines the cyclonic spectra.

stratification is controlled by four items associated with surface wind stress (P_sS^2), barotropic flow (P_mS^2), bed stress ($-D_bS^2$) and interfacial stress($-C_iS^2$), respectively (Formula 14 in their paper). Assuming the coefficients to be same as that in the reference paper, the bulk shear and its contribution items were calculated and shown in Fig. 9. It can be seen that the surface wind stress contribution absolutely dominates with a magnitude more than 3 orders larger than the other three factors (Fig. 9a). The bulk shear increases as the wind direction close to the shear direction and the wind production is positive, while the bulk shear is lower as wind stress production is negative. The direction variation also demonstrates that bulk shear vector (Fig. 9b) rotates clockwise at the local inertial period, with phase close to the near-inertial velocities in the upper mixed layer (14 m) but 180° shift to that in deeper layer below thermocline (70 m), consistent with the phase shift of near-inertial oscillations across the thermocline. The enhancement of shear at the observation is closely related to the near-inertial oscillations induced by the wind.

The near-inertial oscillations induced by winds in the mixed layer can easily excite baroclinic shear instability at the bottom of the mixed layer, and then drive vertical entrainment mixing for energy dissipation (Gardner, 2001). Corresponding to the rapid near-inertial energy decrease in the thermocline in our observations (Fig. 7c,d), the turbulent kinetic energy dissipation rate ε related to near-inertial shear (Fig. 10a) was significantly enhanced with a value above 10^{-7} Wkg^{-1} in the thermocline (Fig. 10c). The baroclinic shear instability probably occurred where the strong near-inertial shear could overcome the background stratification (Fig. 10b) leading to strong entrainment turbulent mixing. The turbulent eddy diffusivity κ_ρ was above 6.3×10^{-5} m^2 s^{-1} in the thermocline, while the larger value above 3.2×10^{-4} m^2 s^{-1} appeared in the upper mixed layer where buoyancy frequency was smaller (Fig. 10d). Fig. 10e and f shows the temporal variations of the dissipation rate ε and turbulent eddy diffusivity κ_ρ. It reveals that the dissipation rate and the eddy diffusivity near the thermocline bottom were a little smaller prior to July 30 as the storm was coming, but increased on August 1– August 2 after the storm, suggesting that the near-inertial mixing delayed the storm forcing.

3.3. Chl-a bloom triggered by Washi

Fig. 11a shows the semi-monthly averaged Chl-*a* concentration prior to the storm (July 12–27) and indicates that the offshore Chl-*a* concentration was relatively low (~0.1 mg m^{-3}) in the northwest SCS. The Chl-*a* concentration significantly increased in the areas along the storm track (white box) and around the mooring-station (yellow box) after the storm (July 28–August 12), and the high concentration also appeared to southeast of Hainan Island (Fig. 11b), which was probably supplied by the nutrient-rich water carried by the increasing runoff from land after storm.

The averages of the Chl-*a* concentrations in the offshore area *A* near the storm track (110–112°E, 17–19°N, white box), area *B* (110–111°E, 17–18°N, black box), nearshore area *C* (111–112°E, 17–19°N, red box), and area *D* near the mooring station (111°48′–112°12′E, 19°23′–19°47′N, yellow box) (Fig. 11b) are chosen to study the variations of Chl-*a* in response to the storm. The results are listed in Table 1, which suggests that the phytoplankton bloom caused by Washi varied spatially and the blooming level was different for different areas. The Chl-*a* concentration after the storm passage increased by 38.5% in all the areas (box *A*), 30.0% in the cooling offshore area (box *C*), and 111.0% to southeast of Hainan Island (box *B*). The Chl-*a* concentration augment induced by the storm was much higher in the near-shore area than that in the

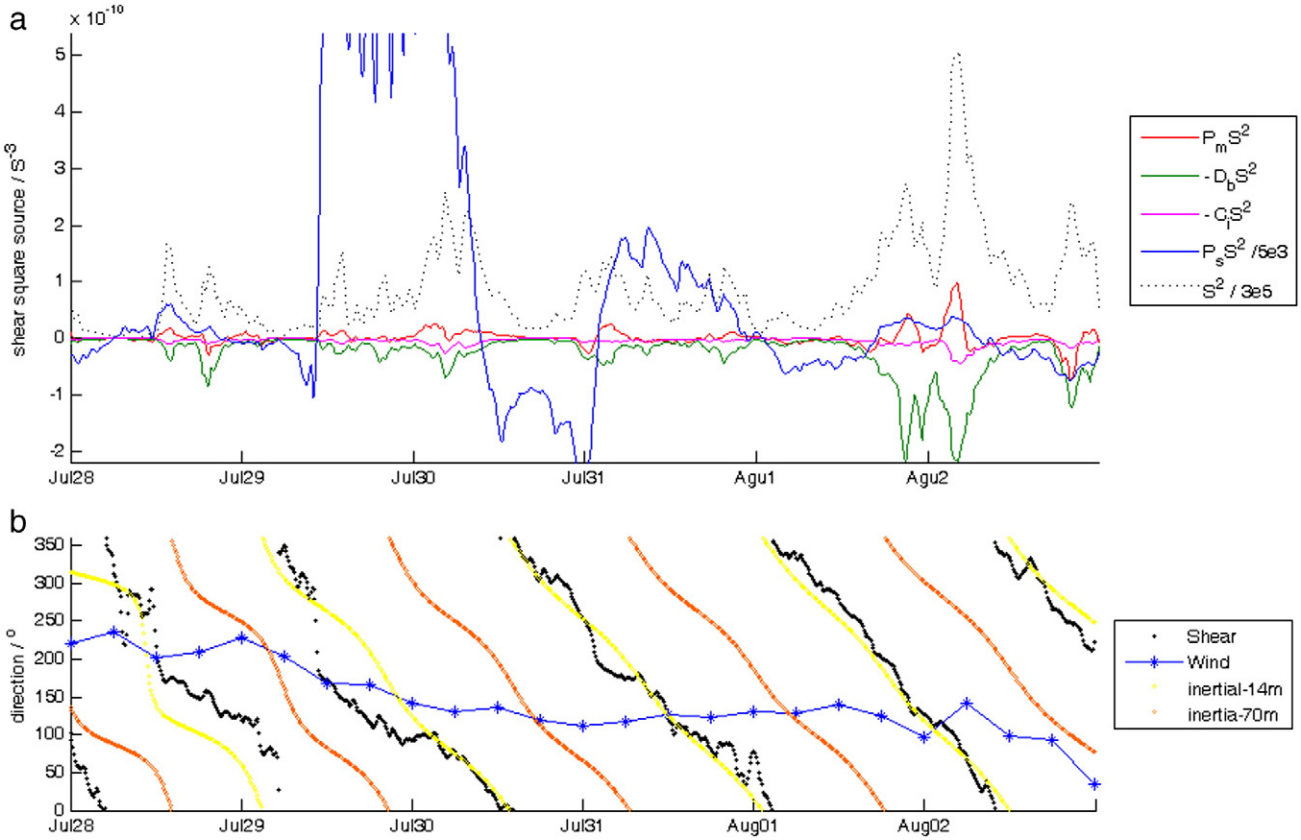

Fig. 9. Bulk properties at the moored station: a) bulk shear squared S^2 (black dash line) and contribution to bulk shear squared from wind stress P_sS^2 (blue line), barotropic effect P_mS^2 (red line), bottom stress $-D_bS^2$ (green line) and interfacial friction $-C_iS^2$ (magenta line). Note the ordered reducing of wind contribution P_sS^2 and the bulk shear S^2. b) directions of bulk shear vector (black dots), wind stress vector (blue star), and local near-inertial velocity vector at 14 m (yellow circle) and 70 m (orange circle). The zero direction with respect to east in an anticlockwise-rotating sense.

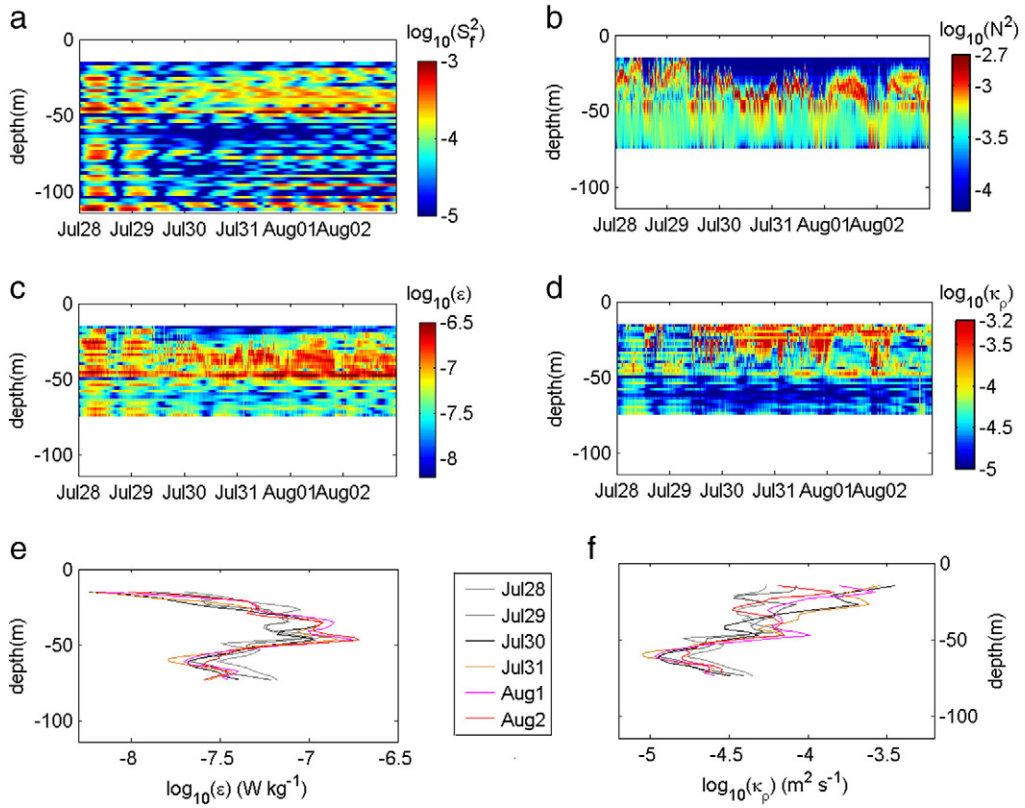

Fig. 10. Profiles of velocity shear log $_{10}(S^2)$ (a), buoyancy frequency $\log_{10}(N^2)$ (b), and turbulent kinetic energy dissipation rate ε (c) and turbulent eddy diffusivity κ_ρ (d). The daily averages of the dissipation rate and the eddy diffusivity are shown in (e) and (f), respectively.

offshore. In the mooring station area, the Chl-*a* concentration was relatively low below 0.1 mg m^{-3} prior to the storm, whereas it increased to above 0.1 mg m^{-3} after the storm. The increasing rate reached as high as ~22.2%.

4. Discussion

The continental shelf is one of the most important areas for land–sea–air interaction and mass-heat transport across the coastal and marginal seas. The shelf area which is only 8% of the total area of the global oceans holds 80% of oceanic biomass (Gattuso et al., 1998), 50% of CO_2 reserves (Thomas et al., 2004), and 28% of primary production (Longhurst et al., 1995) of the global oceans. It plays a crucial role in the vertical nutrient flux maintaining efficient primary productions (Schafstall et al., 2010; Sharples et al., 2007). In the continental shelf region of the SCS, to a large extent, nutrient levels determine phytoplankton productivity. For phytoplankton to grow, the nutrients are normally transported from the deep waters below the thermocline to the upper mixed layer. The storm induced turbulent mixing is one of the major physical processes that enhance upward flux of the deep nutrition

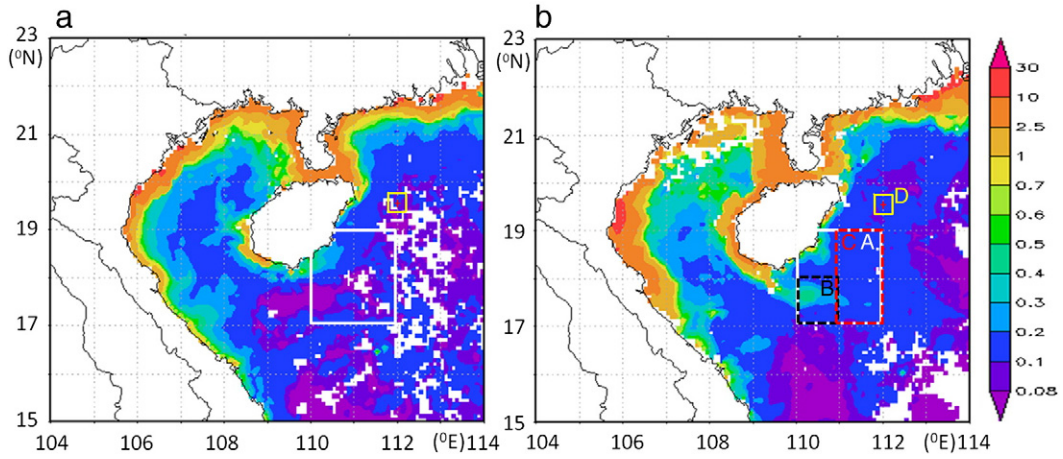

Fig. 11. Chlorophyll-*a* (Chl-*a*) concentration (mg m^{-3}) in Jul–Aug, 2005. Chl-*a* concentration for the pre-storm period averaged from 12 Jul to 27 Jul, 2005 (a); Chl-*a* concentration during the storm averaged from 28 Jul to 11 Aug 2005 (b). Boxes *A* (white), *B* (black), *C* (red), and *D* (yellow) mark the region of (110–112°E, 17–19°N), (110–111°E, 17–18°N), (111–112°E, 17–19°N), and (111°48′–112°12′E, 19°23′–19°47′N) for Chl-*a* averages.

Table 1
Chl-*a* concentrations (mg m^{-3}) in pre- and post-storm based on spatial average for box *A*–*D* in Fig. 11b.

	Box *A*	Box *B*	Box *C*	Box *D*
Pre-storm	0.13	0.10	0.01	0.09
Post-storm	0.18	0.21	0.13	0.11
Chl-*a* increase	38.5%	110.0%	30.0%	22.2%

water to the mixed layer (Lin et al., 2003; Sun et al., 2010; Zheng and Tang, 2007; Zhao et al., 2008).

Washi was a relatively weak tropical storm with only half the strength of a medium storm. Significant phytoplankton blooms, however, were induced as the storm passed through the northwest SCS. The averaged Chl-*a* concentration increased by 38.5% in the storm path and 22.2% in the mooring area 130 km away from the nearest storm center. Euphotic zone with rich nutrients which come from vertical or/and lateral flux is expected for the Chl-*a* increment after the storm. At the mooring station which is more than 100 km from the coast with no plume extending, lateral advection by runoff from land could not play role to enrich the nutrients. The observed total velocity in the mixed layer changes and rotates with time, with the averaged velocity to be north-northwestward of about 0.04 m s^{-1} (Fig. 12). Nutrients could only be advected less than 52 km (about 0.5°) in 15 days with such background velocity. As shown in Fig. 11, the Chl-*a* concentration southeast of the mooring station is lower (<0.1 mg m^{-3}) before the storm, while the Chl-*a* concentration around the station increases to above 0.1 mg m^{-3} after the storm. The lower-concentration advection by the background velocity could not contribute to the phytoplankton bloom around the station. In this paper, we inferred that the turbulent mixing induced by the near-inertial waves was responsible for the vertical nutrient flux. As the near-inertial shear was induced by Washi, strong entrainments occurred in the highly buoyant water below the mixed layer resulting in the enhancement of turbulent mixing. As shown in Fig. 10c, the turbulent kinetic energy was dissipated substantially within the thermocline. Consequently, the enhanced mixing (Fig. 10d) could break up the barrier of the thermocline to flux nutrients from the lower layer water into the surface. The diapycnal flux of nutrients can be calculated by $F_{nutrient} = -\kappa_\rho \frac{\partial C_{nutrient}}{\partial z}$, where $C_{nutrient}$ is the nutrient concentration. For the constant $\frac{\partial C_{nutrient}}{\partial z}$, the nutrient flux is determined by the turbulent eddy diffusivity κ_ρ. During the period of Washi, the turbulent eddy diffusivity κ_ρ increased above 6.3×10^{-5} m^2 s^{-1} in the thermocline and reached 3.2×10^{-4} m^2 s^{-1} in the mixed layer, which was significantly higher than the background turbulent eddy diffusivity of 10^{-5} m^2 s^{-1}. This suggests that the nutrient flux increased by one order of magnitude as influenced by Washi and was mainly a result from the turbulent eddy diffusivity increase rather than the nutrient gradients. In conclusion, the enhanced turbulent mixing induced by the near-inertial waves was responsible for the nutrient flux from nutrient-rich deep waters into the low eutrophic zone, causing the phytoplankton blooms in the continental shelf region southeast of Hainan Island.

5. Conclusion

The observations of ocean current and temperature profiles southeast of Hainan Island under the influence of the tropical storm Washi are reported in this paper, reflecting storm enhanced turbulent mixing and related phytoplankton blooms in the region.

ADCP observations show that strong near-inertial internal waves with the period of 35 h and the maximum current speed above 0.2 m s^{-1} were induced by the strong storm wind. The near-inertial kinetic energy reached a maximum in the upper mixed layer and decreased rapidly beyond the thermocline in which strong velocity shear occurred. Most of the near-inertial energy was dissipated at the bottom of the mixed layer and in the thermocline, and only 11.5% of the energy could penetrate the thermocline and enter the low layer water. The strong shear associated with near-inertial waves enhanced the turbulent mixing with dissipation rate reaching 10^{-7} Wkg^{-1} in the thermocline and the turbulent eddy diffusivity above 3.2×10^{-4} m^2 s^{-1} in the mixed layer.

This study suggests that even a relatively weak tropical storm can also cause phytoplankton blooms in the continental shelf region. The Chl-*a* concentration was normally low in the northwest SCS before the tropical storm in July 2005, and however, it increased above 38% and 22% in the storm area and 130 km away from the storm center, respectively after the passage of Washi. The enhanced nutrient flux through the thermocline was due to the strong mixing induced by the near-inertial internal waves during the passage of Washi, and significantly promoted the phytoplankton productivity in the continental shelf region southeast of Hainan Island.

Acknowledgment

The authors are grateful for the three anonymous reviewers' careful review and constructive suggestions to improve the manuscript. Thanks are given to USA NASA GES DISC for the ocean color data. The work was supported by the National Science Foundation of China (Grant nos. 41176011, 41106012, 40906008, U1133001 and U0933001) and National Science Foundation of Guangdong (Grant no. 925240880100001).

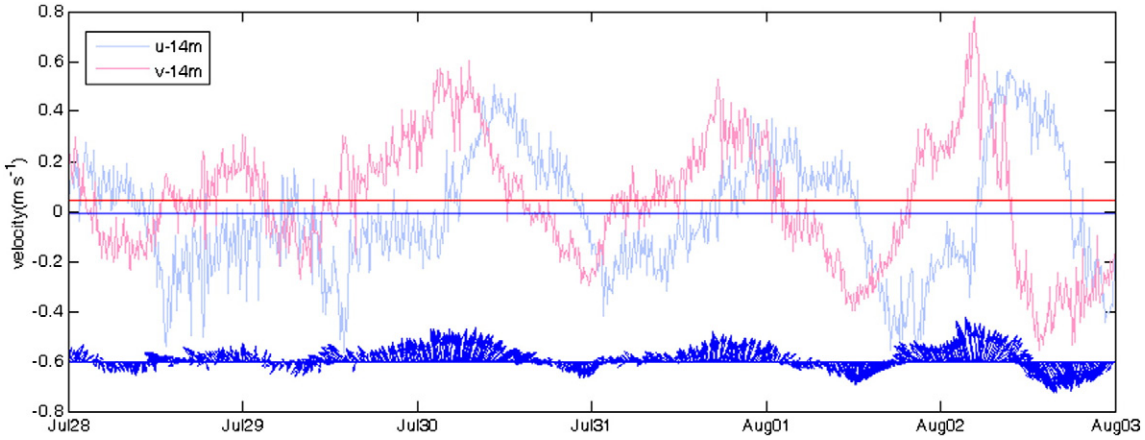

Fig. 12. The ADCP-observed velocity at 14 m in the upper mixed layer, where the straight lines are the time-averaged velocities.

References

Alford, M.H., Gregg, M.C., 2001. Near-inertial mixing: modulation of shear, strain and microstructure at low latitude. J. Geophys. Res. 106 (C8), 16947–16968.

Black, W.J., Dickey, T.D., 2008. Observations and analyses of upper ocean responses to tropical storms and hurricanes in the vicinity of Bermuda. J. Geophys. Res. 113, C08009. http://dx.doi.org/10.1029/2007JC004358.

Burchard, H., Rippeth, T.P., 2009. Generation of bulk shear spikes in shallow stratified tidal seas. J. Phys. Oceanogr. 39, 969–985.

Chant, R.J., 2001. Evolution of near-inertial waves during an upwelling event on the New Jersey Inner Shelf. J. Phys. Oceanogr. 31, 746–764.

Chang, J., Chung, C.-C., Gong, G.-C., 2008a. Influences of cyclones on chlorophyll-*a* concentration and *Synechococcus* abundance in a subtropical western Pacific coastal ecosystem. Mar. Ecol. Prog. Ser. 140, 199–205.

Chang, Y., Liao, H.-T., Lee, M.-A., Chan, J.-W., Shieh, W.-J., Lee, K.-T., Wang, G.-H., Lan, Y.-C., 2008b. Multisatellite observation on upwelling after the passage of Typhoon Hai-Tang in the southern East China Sea. Geophys. Res. Lett. 35, L03612. http://dx.doi.org/10.1029/2007GL032858.

Cui, H., Zhang, S.W., Wang, Q.Y., 2009. Numerical caculation of the response of the South China Sea to typhoon imbudo. Acta Phys. Sin. 58 (9), 6609–6615.

D'Asaro, E.A., 2003. The ocean boundary layer below Hurricane Dennis. J. Phys. Oceanogr. 33, 561–579.

D'Asaro, E.A., Eriksen, C.C., Levin, M.D., Paulson, C.A., Niiler, P., Van Meurs, P., 1995. Upper-ocean inertial currents forced by a strong storm. Part I: data and comparisons with linear theory. J. Phys. Oceanogr. 25, 2909–2935.

Dohan, K., Davis, R.E., 2011. Mixing in the transition layer during two storm events. J. Phys. Oceanogr. 41, 42–66.

Gardner, W.D., 2001. Optics, particles, stratification, and storms on the New England continental shelf. J. Geophys. Res. 106 (C5), 9473–9498.

Gattuso, J.P., Frankignoulle, M., Wollast, R., 1998. Carbon and carbonate metabolism in coastal aquatic ecosystems. Annu. Rev. Ecol. Evol. Syst. 29, 405–434.

Jacob, S.D., Shay, L.K., 2003. The role of oceanic mesoscale features on the tropical cyclone induced mixed layer response. J. Phys. Oceanogr. 33, 649–676.

Lee, C.M., Brink, K.H., 2010. Observations of storm-induced mixing and Gulf Stream Ring incursion over the southern flank of Georges Bank: Winter and summer 1977. J. Geophys. Res. 115, C08008. http://dx.doi.org/10.1029/2009JC005706.

Lin, I.-I., Liu, W.T., Wu, C.-C., Wong, T.F., Hu, C., Chen, Z., Liang, W.-D., Yang, Y., Liu, K.-K., 2003. New evidence for enhanced ocean primary production triggered by tropical cyclone. Geophys. Res. Lett. 30 (13). http://dx.doi.org/10.1029/2003GL017141.

Lin, I.-I., Wu, C.-C., Pun, I.-F., Ko, D.-S., 2008. Upper ocean thermal structure and the western North Pacific category-5 typhoons. Part I: ocean features and category-5 typhoon's intensification. Mon. Weather Rev. 136, 3288–3306.

Longhurst, A., Sathyendranath, S., Platt, T., Caverhill, C., 1995. An estimate of global primary production in the ocean from satellite radiometer data. J. Plankton Res. 17 (6), 1245–1271.

MacKinnon, J.A., Gregg, M.C., 2003. Mixing on the late-summer New England Shelf—solibores, shear and stratification. J. Phys. Oceanogr. 33 (7), 1476–1492.

MacKinnon, J.A., Gregg, M.C., 2005. Spring mixing: turbulence and internal waves during restratification on the New England Shelf. J. Phys. Oceanogr. 35, 2425–2442.

Osborn, T.R., 1980. Estimates of the Local-Rate of Vertical Diffusion from Dissipation Measurements. J. Phys. Oceanogr. 10, 83–89.

Parlmer, M.R., Polton, J.A., Inall, M.E., Rippeth, T.P., Green, J.A.M., Sharples, J., Simpson, J.H., 2013. Variable behavior in pycnocline mixing over shelf seas. Geophys. Res. Lett. (40). http://dx.doi.org/10.1029/2012GL054638.

Palmer, M.R., Rippeth, T.P., Simpson, J.H., 2008. An investigation of internal mixing in a seasonally stratified shelf sea. J. Geophys. Res. 113, C12005. http://dx.doi.org/10.1029/2007JC 004531.

Price, J.F., 1981. Upper ocean response to a hurricane. J. Phys. Oceanogr. 11, 153–175.

Rippth, T.P., Simpson, J.H., Player, R.J., Garcia, M.C., 2002. Current oscillations in the inertial-diurnal band on the Catalonian shelf in spring. Cont. Shelf Res. 22, 247–265.

Rippth, T.P., 2005. Mixing in seasonally stratified shelf seas: a shifting paradigm. Philos. Trans. 363A, 2837–2854.

Sanford, T.B., Price, J.F., Girton, J.B., 2011. Upper-ocean response too Hurricane Frances (2004) observed by profiling EM-APEX floats. J. Phys. Oceanogr. 41, 1041–1056.

Schafstall, J., Dengler, M., Brandt, P., Bange, H., 2010. Tidal induced mixing and diapycnal nutrient fluxes in the Mauritanian region. J. Geophys. Res. 115, C10014. http://dx.doi.org/10.1029/2009JC 005940.

Shang, S., Li, L., Sun, F., Wu, J., Hu, C., Chen, D., Ning, X., Qiu, Y., Zhang, C., Shang, S., 2008. Changes of temperature and bio-optical properties in the South China Sea in response to Typhoon Lingling, 2001. Geophys. Res. Lett. 35, L10602. http://dx.doi.org/10.1029/2008GL033502.

Sharples, J., Tweddle, J.F., Mattias Green, J.A., 2007. Spring-neap modulation of internal tide mixing and vertical nitrate fluxes at the shelf edge in summer. Limnol. Oceanogr. 52 (5), 1735–1747.

Shay, L.K., Peter, G.B., Mariano, A.J., Haking, J.D., Elsberry, R.L., 1992. Upper ocean response to Hurricane Gilbert. J. Geophys. Res. 97 (C12), 20227–20248.

Shearman, R.K., 2005. Observations of near-inertial current variability on the New England shelf. J. Geophys. Res. 110, C02012. http://dx.doi.org/10.1029/2004JC002341.

Shiah, F.-K., Chung, S.-W., Kao, S.-J., Gong, G.-C., Liu, K.-K., 2000. Biological and hydrographical responses to tropical cyclones (typhoons) in the continental shelf of the Taiwan Strait. Cont. Shelf Res. 20, 2029–2044.

Sriver, R.L., Huber, M., 2007. Observational evidence for an ocean heat pump induced by tropical cyclones. Nature 447. http://dx.doi.org/10.1038/nature05785.

Sun, L., Yang, Y.J., Xian, T., Lu, Z.M., Fu, Y.F., 2010. Strong enhancement of chlorophyll-*a* concentration by a weak typhoon. Mar. Ecol. Prog. Ser. 404, 39–50. http://dx.doi.org/10.3354/meps08477.

Sun, Z.Y., Hu, J.Y., Zheng, Q.A., Li, C.Y., 2011. Strong near-inertial oscillations in geostrophic shear in the northern South China Sea. J. Oceanogr. 67, 377–384.

Tang, D.L., Kawamura, H., Doan-Nhu, H., Takahashi, W., 2004b. Remote sensing oceanography of a harmful algal bloom off the coast of southeastern Vietnam. J. Geophys. Res. 109, C03014. http://dx.doi.org/10.1029/2003JC002045.

Tang, D.L., Kawamura, H., Dien, T.-V., Li, M.A., 2004a. Offshore phytoplankton biomass increase and its oceanographic causes in the South China Sea. Mar. Ecol. Prog. Ser. 268, 31–41.

Thomas, H., Bozec, Y., Elkalay, K., de Baar, H.J.W., 2004. Enhanced open ocean storage of CO_2 from shelf sea pumping. Science 304, 1005–1008.

van der Lee, E.M., Umlauf, L., 2011. Internal wave mixing in the Baltic Sea: near-inertial waves in the absence of tides. J. Geophys. Res. 116, C10016.

Wada, A., Niino, H.N., Nakano, H., 2009. Roles of vertical turbulent mixing in the ocean response to Typhoon Rex (1998). J. Oceanogr. 65, 373–396.

Wang, Z.K., DiMarco, S.F., Stössel, M.M., Zhang, X., Howard, M.K., Vall, K., 2012. Oscillation responses to tropical Cyclone Gonu in northern Arabian Sea from a moored observing system. Deep Sea Res. Part I 64, 129–145.

Walker, N.D., 2005. Hurricane-forced upwelling and chlorophyll a enhancement within cold-core cyclones in the Gulf of Mexico. Geophys. Res. Lett. 32, L18610. http://dx.doi.org/10.1029/2005 GL023716.

Wentz, F.J., Gentemann, C., Smith, D., Chelton, D., 2000. Satellite measurements of sea surface temperature through clouds. Science 288, 847–850.

Wu, L., Wang, B., Geng, S., 2005. Growing typhoon influence on east Asia. Geophys. Res. Lett. 32, L18703. http://dx.doi.org/10.1029/2005GL022937.

Zedler, S.E., Dickey, T.D., Doney, S.C., Price, J.F., Yu, X., Mellor, G.L., 2002. Analyses and simulations of the upper ocean's response to Hurricane Felix at the Bermuda Testbed Mooring site: 13–23 August 1995. J. Geophys. Res. 107, C123232. http://dx.doi.org/10.1029/2001JC000969.

Zhou, L., Tian, J.W., Wang, D.X., 2005. The energy distribution of each modes of baroclinic horizontal large-scale wave responding to wind. Sci. China D 35 (10), 997–1006.

Zhao, H., Tang, D.L., Wang, Y.Q., 2008. Comparison of phytoplankton blooms triggered by two typhoons with different intensities and translation speeds in the South China Sea. Mar. Ecol. Prog. Ser. 365, 57–65.

Zhao, H., Tang, D.L., Wang, D.X., 2009. Phytoplankton blooms near the Pearl River Estuary induced by Typhoon Nuri. J. Geophys. Res. 114, C12027. http://dx.doi.org/10.1029/2009JC005384.

Zheng, G.M., Tang, D.L., 2007. Offshore and nearshore chlorophyll increases induced by typhoon winds and subsequent terrestrial rainwater runoff. Mar. Ecol. Prog. Ser. 333, 61–74.

Zheng, Q.A., Ronald, L., Huang, N.E., Pan, J., Liu, W.T., 2006. Observation of ocean current response to 1998 Hurricane Georges in the Gulf of Mexico. Acta Oceanol. Sin. 25 (1), 1–14.